The Astrophysical Journal, 963:53 (11pp), 2024 March 1 https://doi.org/10.3847/1538-4357/ad1a15
© 2024. The Author(s). Published by the American Astronomical Society.
OPEN ACCESS

An Excess of Active Galactic Nuclei Triggered by Galaxy Mergers in MaNGA Galaxies of Stellar Mass $\sim 10^{11}\ M_{\odot}$

Julia M. Comerford[1], Rebecca Nevin[2], James Negus[1], R. Scott Barrows[1], Michael Eracleous[3], Francisco Müller-Sánchez[4], Namrata Roy[5], Aaron Stemo[6], Thaisa Storchi-Bergmann[7], and Dominika Wylezalek[8]
[1] Department of Astrophysical and Planetary Sciences, University of Colorado, Boulder, CO 80309, USA
[2] Fermi National Accelerator Laboratory, P.O. Box 500, Batavia, IL 60510, USA
[3] Department of Astronomy and Astrophysics and Center for Gravitational Wave Physics, The Pennsylvania State University, 525 Davey Lab, University Park, PA 16803, USA
[4] Physics Department, University of Memphis, Memphis, TN 38152, USA
[5] Center for Astrophysical Sciences, Department of Physics and Astronomy, Johns Hopkins University, Baltimore, MD 21218, USA
[6] Department of Physics and Astronomy, Vanderbilt University, Nashville, TN 37235, USA
[7] Departamento de Astronomia, Universidade Federal do Rio Grande do Sul, IF, CP 15051, 91501-970 Porto Alegre, RS, Brazil
[8] Zentrum für Astronomie der Universität Heidelberg, Astronomisches Rechen-Institut, Mönchhofstr, 12-14 D-69120 Heidelberg, Germany
Received 2023 August 31; revised 2023 November 9; accepted 2023 November 10; published 2024 February 28

Abstract

To facilitate new studies of galaxy-merger-driven fueling of active galactic nuclei (AGNs), we present a catalog of 387 AGNs that we have identified in the final population of over 10,000 $z < 0.15$ galaxies observed by the Sloan Digital Sky Survey-IV (SDSS-IV) integral field spectroscopy survey Mapping Nearby Galaxies at Apache Point Observatory (MaNGA). We selected the AGNs via mid-infrared Wide-field Infrared Survey Explorer colors, Swift/Burst Alert Telescope ultra-hard X-ray detections, NRAO Very Large Array Sky Survey and Faint Images of the Radio Sky at Twenty centimeters radio observations, and broad emission lines in SDSS spectra. By combining the MaNGA AGN catalog with a new SDSS catalog of galaxy mergers that were identified based on a suite of hydrodynamical simulations of merging galaxies, we study the link between galaxy mergers and nuclear activity for AGNs above a limiting bolometric luminosity of $10^{44.4}$ erg s^{-1}. We find an excess of AGNs in mergers, relative to nonmergers, for galaxies with stellar mass $\sim 10^{11}\ M_{\odot}$, where the AGN excess is somewhat stronger in major mergers than in minor mergers. Further, when we combine minor and major mergers and sort by merger stage, we find that the highest AGN excess occurs in post-coalescence mergers in the highest-mass galaxies. However, we find no evidence of a correlation between galaxy mergers and AGN luminosity or accretion rate. In summary, while galaxy mergers overall do appear to trigger or enhance AGN activity more than nonmergers, they do not seem to induce higher levels of accretion or higher luminosities. We provide the MaNGA AGN Catalog and the MaNGA Galaxy Merger Catalog for the community here.

Unified Astronomy Thesaurus concepts: Active galactic nuclei (16); Active galaxies (17); Radio active galactic nuclei (2134); X-ray active galactic nuclei (2035); Galaxy mergers (608); Galaxy interactions (600)

Supporting material: machine-readable tables

1. Introduction

Nearly all massive galaxies are thought to host central supermassive black holes (SMBHs; Kormendy & Richstone 1995; Ferrarese & Ford 2005), and these SMBHs build up their mass by accreting gas as active galactic nuclei (AGNs). The main avenues for driving gas accretion onto SMBHs are secular processes internal to galaxies (e.g., Lynden-Bell 1979; Combes & Gerin 1985; Bournaud & Combes 2002) and tidal torques induced during galaxy mergers that cause gas to lose its angular momentum and infall to galaxy centers (e.g., Barnes & Hernquist 1991; Springel et al. 2005; Hopkins & Hernquist 2009). However, the relative roles and importances of these two mechanisms for driving SMBH growth remain unclear. Observational studies disagree on fundamental questions such as whether AGNs are more often found in galaxy mergers (e.g., Canalizo & Stockton 2001; Villar-Martín et al. 2011; Ellison et al. 2019; Araujo et al. 2023; Pierce et al. 2023) or not (e.g., Dunlop et al. 2003; Gabor et al. 2009; Cisternas et al. 2011).

The reason for the disagreement may be that the role of galaxy mergers in triggering AGNs also depends on factors such as galaxy-merger mass ratio, galaxy-merger stage, AGN luminosity, and accretion rate. For example, some theoretical work has suggested that major mergers of galaxies preferentially trigger AGNs (e.g., Barnes & Hernquist 1992; Hopkins & Hernquist 2009; Capelo et al. 2017), though the observations have not yet converged on a conclusion (e.g., Glikman et al. 2015; Villforth et al. 2017; Marian et al. 2019).

Further, simulations predict that SMBH activity peaks in late-stage (often defined as, for example, <10 kpc bulge separation) galaxy mergers (Di Matteo et al. 2005; Springel et al. 2005; Capelo et al. 2015), but the observations have been limited by only handfuls of known late-stage mergers hosting AGNs (e.g., Koss et al. 2012; Comerford et al. 2015; Barrows et al. 2016). To further complicate the picture, other observations suggest that SMBH activity peaks in post-coalescence mergers (e.g., Ellison et al. 2013; Satyapal et al. 2014).

Meanwhile, galaxy simulations have also found that more luminous AGNs are preferentially triggered by galaxy-merger-

Original content from this work may be used under the terms of the Creative Commons Attribution 4.0 licence. Any further distribution of this work must maintain attribution to the author(s) and the title of the work, journal citation and DOI.

driven inflows of gas, while less luminous AGNs are preferentially fueled by the stochastic accretion of gas outside of mergers (e.g., Hopkins et al. 2014; Capelo et al. 2015). Currently, the observations are in tension about whether galaxy mergers preferentially trigger the most luminous AGNs (e.g., Treister et al. 2012; Glikman et al. 2015) or whether there is no correlation of mergers with AGN luminosity (e.g., Kocevski et al. 2012; Villforth et al. 2014). The question of whether galaxy mergers fuel higher accretion rates onto SMBHs also remains relatively untested (e.g., Marian et al. 2019).

A powerful tool for addressing these open questions on the roles of galaxy mergers in triggering AGNs at low redshifts is the Sloan Digital Sky Survey-IV (SDSS-IV) survey Mapping Nearby Galaxies at Apache Point Observatory (MaNGA), which enables spatially resolved studies of galaxies in unprecedented numbers (over 10,000 $z < 0.15$ galaxies; Bundy et al. 2015; Law et al. 2015). Here, we lay the groundwork for such analyses by first building a catalog of AGNs in MaNGA, which we identify with mid-infrared, X-ray, radio, and broad-emission-line observations. This is an expansion of the catalog presented for an earlier MaNGA data release in Comerford et al. (2020). We also present a catalog of galaxy mergers in MaNGA that were identified based on a suite of hydrodynamical simulations of galaxy mergers, where the identifications include major and minor mergers as well as early-stage, late-stage, and post-coalescence mergers. We combine our AGN catalog with the galaxy-merger catalog to study the role of mergers in triggering AGNs as a function of merger mass ratio, merger stage, AGN luminosity, and SMBH accretion rate. Future work will focus on the spatially resolved impacts of mergers on galaxies, including spatially resolved star formation rates and star formation histories.

This paper is organized as follows. In Section 2, we present the parent sample of MaNGA galaxies and their properties. In Section 3, we present the catalog of 387 AGNs in MaNGA, which we identified using Wide-field Infrared Survey Explorer (WISE) mid-infrared color cuts, Swift/Burst Alert Telescope (BAT) hard X-ray sources, NRAO Very Large Array Sky Survey (NVSS)/Faint Images of the Radio Sky at Twenty centimeters (FIRST) 1.4 GHz radio sources, and SDSS broad emission lines. Section 4 describes how the galaxy mergers in MaNGA are identified. In Section 5, we present and discuss our results, which indicate an excess of AGNs in galaxy mergers, when compared to nonmergers, in the moderate- to high-mass galaxies in our sample. Finally, Section 6 summarizes our conclusions.

We assume a Hubble constant $H_0 = 70\,\mathrm{km\,s^{-1}\,Mpc^{-1}}$, $\Omega_m = 0.3$, and $\Omega_\Lambda = 0.7$ throughout, and all distances are given in physical (not comoving) units.

2. MaNGA Galaxy Sample

MaNGA is an SDSS-IV integral field spectroscopy survey of $0.01 < z < 0.15$ (average redshift $z = 0.03$) galaxies, and its final catalog consists of over 10,000 unique galaxies (Bundy et al. 2015; Drory et al. 2015; Law et al. 2015; Yan et al. 2016; Blanton et al. 2017; Wake et al. 2017; Abdurro'uf et al. 2022). MaNGA uses 2″ fibers grouped into hexagonal bundles, which range in diameter from 12.″5 to 32.″5. The observations span 3600–10300 Å with a spectral resolving power of $R \sim 2000$. The point-spread function FWHM is 2.″5, corresponding to physical resolutions of 0.5–6.5 kpc for its redshift range. MaNGA targets galaxies with stellar masses $>10^9\ M_\odot$, and the mass distribution is designed to be flat (Yan et al. 2016). In addition, the MaNGA survey was designed to spectroscopically map galaxies out to at least 1.5 times the effective radius, and the typical MaNGA galaxy is mapped out to a radius of ∼15 kpc.

Here, we use the final catalog of galaxies in MaNGA, which was released in the eleventh MaNGA Product Launch (MPL-11; Abdurro'uf et al. 2022). Our analyses rely on galaxy properties provided in the Pipe3D Value Added Catalog (Sánchez et al. 2016, 2018), including redshift and galaxy stellar mass.

3. MaNGA AGN Catalog

We provide here a catalog of 387 AGN identifications in the full, final population of MaNGA galaxies. The properties presented in our catalog are shown in Table 1. We select the AGNs in a similar fashion to Comerford et al. (2020), which searched for AGNs in the 6261 MaNGA galaxies in MPL-8.

We select AGNs using four different data sets, where each data set has full coverage of the MaNGA field and therefore could potentially detect AGNs in all MaNGA galaxies. The four approaches that we use are WISE mid-infrared color cuts, Swift/BAT hard X-ray sources, NVSS/FIRST 1.4 GHz radio sources, and SDSS broad emission lines. We outline each approach below.

3.1. WISE Mid-infrared Colors

Mid-infrared emission from the hot dust in the obscuring structure around AGNs is a useful selector for both obscured and unobscured AGNs. Here, we select AGNs using WISE mid-infrared observations of the MaNGA catalog of galaxies. WISE observed the full sky in four bands at 3.4, 4.6, 12, and 22 μm ($W1$, $W2$, $W3$, and $W4$, respectively). We cross-match the AllWISE Source Catalog (Wright et al. 2010; Mainzer et al. 2014) to the MaNGA galaxies using a matching radius of 6.″25, which is the smallest radius of a MaNGA integral field unit. As in Comerford et al. (2020), we select AGNs using the 75% reliability criteria of $W1 - W2 > 0.486 \exp\{0.092(W2 - 13.07)^2\}$ and $W2 > 13.07$, or $W1 - W2 > 0.486$ and $W2 \leqslant 13.07$ (Assef et al. 2018), which yields 130 AGNs.

To determine the bolometric luminosity of each WISE AGN, we estimate the rest-frame 6 μm luminosity and convert it to the rest-frame 2–10 keV luminosity using the correlation from Stern (2015). Then, we convert the rest-frame 2–10 keV luminosity to the bolometric luminosity by multiplying by a factor of 20, which is a typical bolometric correction for AGNs (e.g., Elvis et al. 1994; Marconi et al. 2004).

3.2. Swift/BAT Ultra-hard X-Rays

Hard X-rays are excellent tracers of the hot X-rays that originate close to AGN accretion disks. The Swift observatory's BAT is carrying out a uniform all-sky survey in the ultra-hard X-ray (14–195 keV), and the 105 month BAT catalog, which includes AGN identifications (Oh et al. 2018), has already been cross-matched to Data Release 12 (DR12) of the SDSS (Alam et al. 2015). SDSS DR12 includes all of the MaNGA galaxies, and we find that there are 30 BAT-identified AGNs in MaNGA.

For these 30 BAT AGNs, we convert the published 14–195 keV luminosities to bolometric luminosities using the bolometric correction $L_{\mathrm{bol}}/L_{14-195\,\mathrm{keV}} = 8.47$ (Ricci et al. 2017; Ichikawa et al. 2019).

Table 1
Data Fields in the MaNGA AGN Catalog

No.	Field	Description
1	MANGA_ID	Galaxy identifier assigned by MaNGA
2	R.A.	R.A. of MaNGA galaxy (J2000, decimal degrees)
3	decl.	decl. of MaNGA galaxy (J2000, decimal degrees)
4	Z	Spectroscopic redshift of galaxy
5	WISE_AGN	Whether AGN was selected in WISE (Boolean)
6	LOG_LBOL_WISE	Log bolometric luminosity of WISE AGN (erg s^{-1})
7	LOG_LBOL_WISE_ERR	Log bolometric luminosity error of WISE AGN (erg s^{-1})
8	BAT_AGN	Whether AGN was selected in BAT (Boolean)
9	LOG_LBOL_BAT	Log bolometric luminosity of BAT AGN (erg s^{-1})
10	LOG_LBOL_BAT_ERR	Log bolometric luminosity error of BAT AGN (erg s^{-1})
11	RADIO_AGN	Whether AGN was selected in NVSS/FIRST (Boolean)
12	RADIO_CLASS	Quasar-mode (HERG) or radio-mode (LERG)
13	LOG_LBOL_RADIO	Log bolometric luminosity of NVSS/FIRST AGN (erg s^{-1})
14	LOG_LBOL_RADIO_ERR	Log bolometric luminosity error of NVSS/FIRST AGN (erg s^{-1})
15	BROAD_AGN	Whether AGN was selected by broad lines (Boolean)
16	LOG_LBOL_BROAD	Log bolometric luminosity of broad-line AGN (erg s^{-1})
17	LOG_LBOL_BROAD_ERR	Log bolometric luminosity error of broad-line AGN (erg s^{-1})

Note. The MaNGA AGN Catalog is available in its entirety in FITS format from the original publisher.

(This table is available in its entirety in machine-readable form.)

3.3. NVSS/FIRST 1.4 GHz Radio Sources

Radio jet emission is another useful indicator of AGNs. Radio AGNs in SDSS Data Release 7 (DR7) have been identified from NVSS (Condon et al. 1998) and FIRST (Becker et al. 1995) observations. NVSS is a 1.4 GHz continuum survey that fully covers the sky north of a decl. of −40 deg, while FIRST is a 1.4 GHz survey of 10,000 square degrees of the North and South Galactic Caps. Using these two surveys, Best & Heckman (2012) created an SDSS DR7 radio source catalog with a flux density limit of 5 mJy, which extends down to a 1.4 GHz radio luminosity of $\sim 10^{23}$ W Hz^{-1} at $z = 0.1$. SDSS DR17 includes all of the MaNGA galaxies, and we cross-match to the Best & Heckman (2012) catalog here.

In their analysis, Best & Heckman (2012) separated the radio sources into the two classes of high-excitation radio galaxies (HERGs) and low-excitation radio galaxies (LERGs). Building on a library of optical diagnostics (e.g., Kewley et al. 2006; Cid Fernandes et al. 2010), they used optical emission lines detected in the SDSS spectra to make these classifications. Then, Best & Heckman (2012) further separated the radio sources into either star-forming galaxies or radio-loud AGNs. They did so using the relationship between the 4000 Å break strength and the ratio of the radio luminosity to the galaxy stellar mass (Best et al. 2005), Baldwin–Philips–Terlevich (BPT; Baldwin et al. 1981) line flux ratio diagnostics, and the relationship between Hα luminosity and radio luminosity. By cross-matching their AGN classifications to MaNGA, we find 221 radio AGNs detected in MaNGA.

Then, we convert the 1.4 GHz integrated fluxes of the sources to 2–10 keV luminosities via the scaling relation in Panessa et al. (2015), and apply the same bolometric correction as in Section 3.1.

3.4. Broad Emission Lines

Broad Balmer emission lines trace Type 1 AGNs, as the broad lines are produced in the high-density, and high-velocity, gas very close to the SMBH (e.g., Osterbrock 1991). Oh et al. (2015) analyzed the spectra of SDSS DR7 galaxies at $z < 0.2$ for evidence of broad Hα emission lines, which they used to build a catalog of Type 1 AGNs in SDSS DR7. We cross-match their catalog with MaNGA, since all MaNGA galaxies are included in SDSS DR7, and we find 78 broad-line AGNs in MaNGA.

We then convert the [O III] λ5007 luminosities given in Oh et al. (2015) to bolometric luminosities via the scaling relation of Pennell et al. (2017).

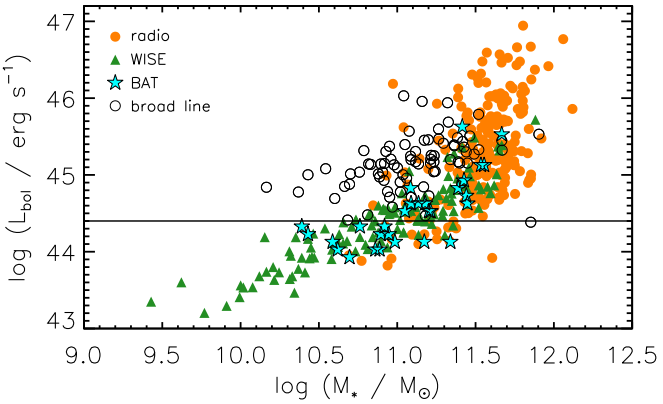

Figure 1. Comparison between AGN bolometric luminosities and host-galaxy stellar masses for the NVSS/FIRST radio-selected (orange filled circles), WISE-selected (green triangles), Swift/BAT-selected (cyan stars), and SDSS broad-line-selected (open black circles) AGNs in MaNGA. Since each survey has a different sensitivity, we employ a limiting AGN bolometric luminosity of $\log(L_{bol}/\mathrm{erg\ s^{-1}}) > 44.4$ (horizontal line) for the analyses in this paper. All four approaches can detect AGNs above this detection limit.

3.5. Comparison of AGN Selectors

We compare the AGN bolometric luminosities and host-galaxy stellar masses of the MaNGA AGNs in Figure 1. Several well-known trends and selection biases are apparent in our sample of AGNs. First, the overall trend of increasing AGN bolometric luminosity with host-galaxy stellar mass is due to the SMBH mass rising with the bulge stellar mass (e.g.,

Magorrian et al. 1998), since AGN luminosity correlates with Eddington luminosity, which correlates with SMBH mass.

Further, there are biases in the AGN selectors. For example, WISE-selected AGNs preferentially reside in lower-stellar-mass galaxies, since the infrared light from the AGN typically dominates over that from star formation in low-mass galaxies, which have relatively low star formation rates compared to high-mass galaxies (e.g., Mendez et al. 2013; Barrows et al. 2021). Meanwhile, radio-selected AGNs are biased toward higher-stellar-mass galaxies (e.g., Baum et al. 1992; Véron-Cetty & Véron 2001; Kauffmann et al. 2008), which could be because radio AGNs are a last phase in the evolution of AGNs when the host galaxies have already slowed their star formation (e.g., Comerford et al. 2020).

To account for such biases, it is good practice to use mass-matched control samples or to bin the AGNs in this catalog by galaxy stellar mass, as we do in the analyses that follow.

Finally, each telescope and survey that was used to detect the AGNs has a different sensitivity, which introduces a bias when combining the AGNs identified by different approaches. To combat this bias, we employ a limiting AGN bolometric luminosity of $\log(L_{\rm bol}/{\rm erg\ s^{-1}}) > 44.4$, above which all four approaches can detect an AGN. This luminosity cutoff decreases our AGN sample size from 387 to 301. This excludes 50%, 48%, 8%, and 1% of the Swift/BAT, WISE, radio, and broad-line AGNs, respectively. The remaining 301 AGNs, all of which are detected at $\log(L_{\rm bol}/{\rm erg\ s^{-1}}) > 44.4$, are the population we use in the analyses that follow.

4. MaNGA Galaxy Merger Catalog

To identify the galaxy mergers in the MaNGA catalog of galaxies, we used the SDSS galaxy classifications of Nevin et al. (2023). They identified galaxy mergers using a linear discriminant analysis of seven individual imaging predictors (Gini, M_{20}, concentration, asymmetry, clumpiness, Sérsic index, and shape asymmetry) that they measured for mock SDSS r-band images (Nevin et al. 2019). The mock SDSS r-band images were created from a suite of hydrodynamical simulations of merging and isolated galaxies that were then processed with a dust radiative-transfer code. Nevin et al. (2023) then applied the linear discriminant analysis classifier to the r-band images of the SDSS Data Release 16 (DR16) photometric sample of galaxies to determine the probability that each galaxy is an early-stage major merger, early-stage minor merger, late-stage major merger, late-stage minor merger, post-coalescence major merger, and post-coalescence minor merger. Each probability is calculated independently, and more detail is provided in Nevin et al. (2023).

Here, major mergers are defined as galaxies with mass ratios $\mu \geqslant 1/4$, whereas minor mergers are defined as galaxies with mass ratios $\mu < 1/4$. Early-stage mergers are defined as mergers roughly between first pericentric passage and apocentric passage (where the average separation of the two stellar bulges drops down to 10 kpc; Nevin et al. 2019), late-stage mergers are defined as mergers roughly between apocentric passage and coalescence, and post-coalescence mergers are defined as the stage from coalescence until 0.5 or 1 Gyr after coalescence. In this paper, we use the 1 Gyr after coalescence classification for post-coalescence mergers, because, as Nevin et al. (2023) point out, IllustrisTNG galaxies exhibit disturbed morphologies for up to 2.5 Gyr following a merger (Bickley et al. 2021).

The accuracies of the early-stage, late-stage, and post-coalescence major merger classifications are 0.86, 0.94, and 0.90, respectively, and the precisions are 0.95, 0.97, and 0.94, respectively (Nevin et al. 2023). The merger classification methodology performs best when applied in bulk to large populations like the MaNGA sample here, rather than to individual galaxies.

First, we match the full catalog of MaNGA galaxies to the Nevin et al. (2023) SDSS DR16 galaxy classification catalog using a cross-match radius of 20″. We choose this radius because it corresponds to 12 kpc at the median redshift of MaNGA and 50 kpc at the highest redshift of MaNGA, and galaxies matched within 50 kpc have been well-established to be likely merging pairs (e.g., Patton et al. 2002; Ellison et al. 2011; Snyder et al. 2017). We find that 7669 of the MaNGA galaxies (76%) match within this radius, are photometrically clean (no photometric flags, where the three possible photometric flags are "low S/N," "outlier predictor," and "segmap"; see Section 2.2 of Nevin et al. 2023), and have morphology classifications that we can use in our analyses. We provide the MaNGA Galaxy Merger Catalog here, which gives classification probabilities for these 7669 MaNGA galaxies. We ultimately classify some of these galaxies as mergers and some as nonmergers, as detailed below. The data fields in the catalog are described in Table 2.

In our analyses, we follow the practice recommended in Nevin et al. (2023) to identify mergers and nonmergers. We use the merger probability values from the marginalized analysis that corresponds to the 50th percentile of the probability distribution for each individual galaxy. We use a probability threshold of 0.5 to distinguish between mergers and mergers. The galaxy mergers are those where `p_merg_stat_50_major_merger` or `p_merg_stat_50_minor_merger` is greater than 0.5, and the corresponding nonmergers are those where `p_merg_stat_50_major_merger` and `p_merg_stat_50_minor_merger` are less than 0.5.

Major mergers are those where `p_merg_stat_50_major_merger` is greater than 0.5, and `p_merg_stat_50_major_merger` is greater than `p_merg_stat_50_minor_merger`. Similarly, minor mergers are those where `p_merg_stat_50_minor_merger` is greater than 0.5, and `p_merg_stat_50_minor_merger` is greater than `p_merg_stat_50_major_merger`.

For each galaxy, there are six merger stage probabilities in total. To determine merger stage, we compare the merger probabilities (calculated separately for major and minor mergers) for each stage (early stage, late stage, and post-coalescence). For example, early-stage mergers are those where `p_merg_stat_50_major_merger_early` or `p_merg_stat_50_minor_merger_early` is greater than 0.5, and either `p_merg_stat_50_major_merger_early` or `p_merg_stat_50_minor_merger_early` is greater than the probabilities of all the other merger stages (`p_merg_stat_50_major_merger_late`, `p_merg_stat_50_minor_merger_late`, `p_merg_stat_50_major_merger_postc_include_coal_1_0`, and `p_merg_stat_50_minor_merger_postc_include_coal_1_0`). If none of the six merger stage probabilities exceed 0.5, then we classify the galaxy as a nonmerger. Overall, most probability values are either at the low (0) or the high (1) end of the distribution (Nevin et al. 2023).

Table 2
Data Fields in the MaNGA Galaxy Merger Catalog

No.	Field	Description
1	ObjID	SDSS ObjID from DR16
2	RAdeg-MaNGA	R.A. in the MaNGA catalog (J2000, decimal degrees)
3	DEdeg-MaNGA	decl. in the MaNGA catalog (J2000, decimal degrees)
4	RAdeg-SDSS	R.A. in the SDSS catalog (J2000, decimal degrees)
5	DEdeg-SDSS	decl. in the SDSS catalog (J2000, decimal degrees)
6	low S/N	Photometric flag, value is 1 if thrown. See N23 for more details on the three photometric flags. The "low S/N" flag is thrown when the average S/N value is below 2.5.
7	outlier predictor	Same as above, the "outlier predictor" flag is thrown when one or more imaging predictors from the LDA classification are outside the range of predictor values from the simulated galaxies.
8	segmap	Same as above, the "segmap" flag is thrown when the segmentation map used for imaging analysis does not include the central pixel or for when the segmentation map extends beyond the edge of a clipped image.
9	p_merg_stat_16_major_merger	Merger probability value from the marginalized analysis that corresponds to the 16th percentile of the probability distribution for this individual galaxy for the major merger overall (all stages) classification
10	p_merg_stat_50_major_merger	Same as above but for the 50th percentile, or median of the probability distribution for the major merger overall (all stages) classification
11	p_merg_stat_84_major_merger	Same as above but for the 84th percentile for the major merger overall (all stages) classification
12	cdf_major_merger	Cumulative distribution function value that corresponds to the 50th percentile probability value given above. The full details of this calculation are in N23. Briefly, this value is useful for comparing how an individual galaxy's p_merg_50 value compares to all SDSS galaxies classified using the same classification.
13	p_merg_stat_16_major_merger_early	Same as above but for the classification that identifies major mergers in the early stage
14	p_merg_stat_50_major_merger_early	
15	p_merg_stat_84_major_merger_early	
16	cdf_major_merger_early	
17	p_merg_stat_16_major_merger_late	Same as above but for the classification that identifies major mergers in the late stage
18	p_merg_stat_50_major_merger_late	
19	p_merg_stat_84_major_merger_late	
20	cdf_major_merger_late	
21	p_merg_stat_16_major_merger_prec	Same as above but for the classification that identifies major mergers in the early and late stages (pre-coalescence)
22	p_merg_stat_50_major_merger_prec	
23	p_merg_stat_84_major_merger_prec	
24	cdf_major_merger_prec	
25	p_merg_stat_16_major_merger_postc_include_coal_0.5	Same as above but for the classification that identifies major mergers in the post-coalescence stage, where the merger is defined to end 0.5 Gyr after coalescence
26	p_merg_stat_50_major_merger_postc_include_coal_0.5	
27	p_merg_stat_84_major_merger_postc_include_coal_0.5	
28	cdf_major_merger_postc_include_coal_0.5	
29	p_merg_stat_16_major_merger_postc_include_coal_1.0	Same as above but for the classification that identifies major mergers in the post-coalescence stage, where the merger is defined to end 1.0 Gyr after coalescence
30	p_merg_stat_50_major_merger_postc_include_coal_1.0	
31	p_merg_stat_84_major_merger_postc_include_coal_1.0	
32	cdf_major_merger_postc_include_coal_1.0	
33	p_merg_stat_16_minor_merger	Same as above but for the minor merger classifications
34	p_merg_stat_50_minor_merger	
35	p_merg_stat_84_minor_merger	
36	cdf_minor_merger	
37	p_merg_stat_16_minor_merger_early	
38	p_merg_stat_50_minor_merger_early	
39	p_merg_stat_84_minor_merger_early	
40	cdf_minor_merger_early	
41	p_merg_stat_16_minor_merger_late	
42	p_merg_stat_50_minor_merger_late	
43	p_merg_stat_84_minor_merger_late	
44	cdf_minor_merger_late	
45	p_merg_stat_16_minor_merger_prec	

Table 2
(Continued)

No.	Field	Description
46	p_merg_stat_50_minor_merger_prec	
47	p_merg_stat_84_minor_merger_prec	
48	cdf_minor_merger_prec	
49	p_merg_stat_16_minor_merger_postc_include_coal_0.5	
50	p_merg_stat_50_minor_merger_postc_include_coal_0.5	
51	p_merg_stat_84_minor_merger_postc_include_coal_0.5	
52	cdf_minor_merger_postc_include_coal_0.5	
53	p_merg_stat_16_minor_merger_postc_include_coal_1.0	
54	p_merg_stat_50_minor_merger_postc_include_coal_1.0	
55	p_merg_stat_84_minor_merger_postc_include_coal_1.0	
56	cdf_minor_merger_postc_include_coal_1.0	

Note. More details are given for the derivation of all columns in Nevin et al. (2023). The MaNGA Galaxy Merger Catalog is available in its entirety in FITS format from the original publisher.

(This table is available in its entirety in machine-readable form.)

We note that the merger stage classifications have more false negatives (are more contaminated by other merger stages) than the major versus minor merger classifications (Nevin et al. 2023), which leads to fewer galaxies in each classification bin. Due to small number statistics, this results in larger error bars in the merger stage analyses that follow (e.g., Section 5.2).

To account for the bias that galaxy mergers are preferentially found in higher-mass galaxies (Figure 2), we bin by galaxy stellar mass in the analyses that follow.

5. Results and Discussion

5.1. An Excess of AGNs in Galaxy Mergers of Stellar Mass $\sim 10^{11}$ $M_\odot$

Overall, we find that $4.2\% \pm 0.3\%$ (168/3969) of galaxy mergers host AGNs and $1.8\% \pm 0.2\%$ (66/3700) of nonmergers host AGNs with $\log(L_{\rm bol}/{\rm erg\ s^{-1}}) > 44.4$ in MaNGA. For comparison, another study of AGN fractions in MaNGA galaxies, which used close galaxy pairs to define the merger sample, found that 23.8% of mergers host AGNs while 14.5% of nonmergers host AGNs (Fu et al. 2018). The higher AGN fractions in that study are likely explained by the difference in AGN luminosity range ($41 \sim \lesssim \log(L_{\rm bol}/{\rm erg\ s^{-1}}) \sim \lesssim 45$ for Fu et al. 2018) as well as the difference in AGN selection; Fu et al. (2018) selected AGNs via a combination of the [O III]/Hβ versus [N II]/Hα BPT diagnostic (Baldwin et al. 1981) and the Hα equivalent width versus [N ii]/Hα (WHAN; Cid Fernandes et al. 2010) diagnostic. Such AGN diagnostics have known issues with misclassification, since the relevant emission-line ratio values can be changed by emission from shocks, young hot stars, and evolved hot stars (e.g., Rich et al. 2011; Kewley et al. 2013; Albán & Wylezalek 2023). Our AGN classifications via mid-infrared, hard X-ray, radio, and broad emission lines are inherently more conservative.

Since the AGN fraction and merger fraction are correlated with host-galaxy stellar mass, we also examine the fraction of AGNs in mergers, $f_{\rm AGN}$, as compared to nonmergers within the same galaxy stellar mass bins. Using galaxy stellar mass bins of 0.5 dex centered at $\log(M_*/M_\odot) = [10.75, 11.25, 11.75]$, we measure $f_{\rm AGN}$ in each mass bin for the major mergers, minor mergers, and nonmergers. We reproduce the well-known trend of the AGN fraction increasing with host-galaxy stellar mass, for each galaxy type (Figure 3, top panel). In each galaxy stellar mass bin, we find that the AGN fraction trends higher in the major mergers than in the minor mergers. By comparing the fraction of AGNs in mergers to the fraction of AGNs in mass-matched nonmergers, we find that there is an AGN excess in major mergers and in minor mergers in the galaxy stellar mass bin $11 < \log(M_*/M_\odot) < 11.5$ (Figure 3, bottom panel). The excess for major mergers is a factor of 1.8, and the excess for minor mergers is a factor of 1.5.

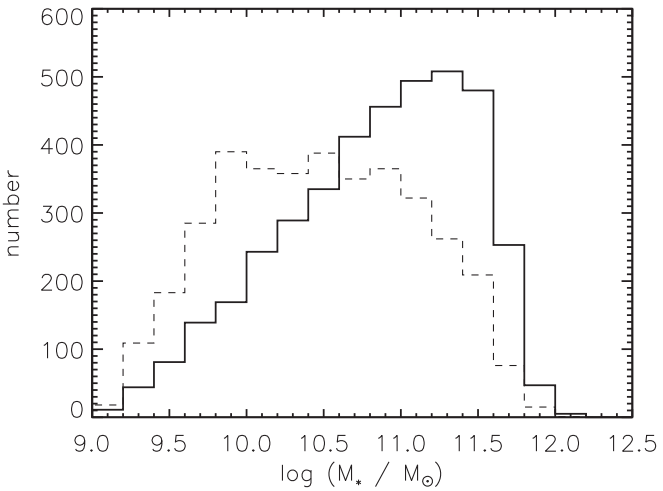

Figure 2. Comparison of host-galaxy stellar masses for the mergers (solid histogram) and nonmergers (dashed histogram) in MaNGA.

This effect was predicted in cosmological hydrodynamical simulations that examined the AGN fraction in major mergers at a range of redshifts (McAlpine et al. 2020). That study only used AGNs with bolometric luminosities $L_{\rm bol} \geqslant 10^{43}$ erg s^{-1}, which encompasses all of our MaNGA AGNs. In their lowest-redshift bin ($0 < z < 1$) they found the greatest excess of AGNs triggered by major mergers in moderate-mass galaxies ($\log(M_*/M_\odot) \sim$ 10–11), and no AGN excess at higher galaxy masses. Our observations match these predictions.

Our results are also broadly consistent with the AGN excesses observed in other studies at similar redshift ranges. A MaNGA study of galaxy pairs, where the AGNs were selected by BPT and WHAN diagnostics, found that for 10 kpc separation galaxy pairs the rate of stochastic fueling was enhanced by a factor of 1.3 (Steffen et al. 2023). They found no

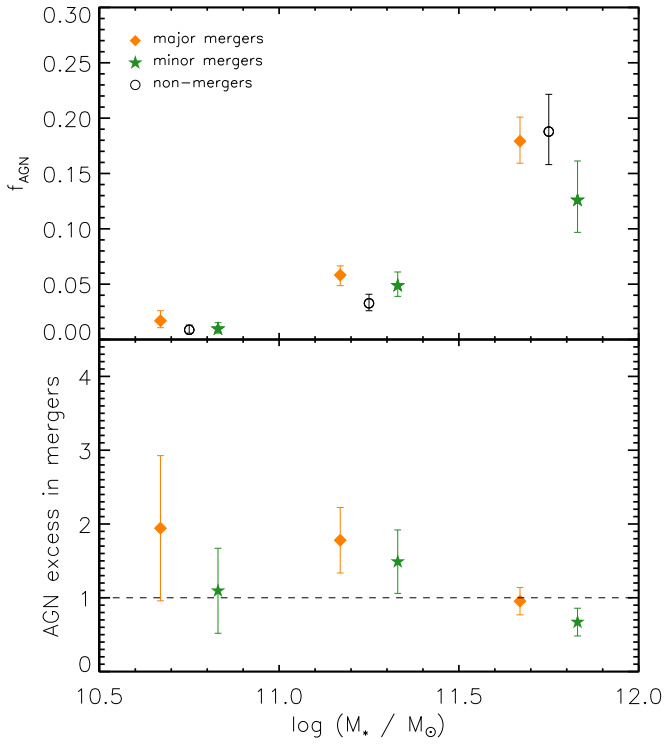

Figure 3. The fraction of galaxies that host AGNs and the AGN excess as a function of galaxy stellar mass, for different mass ratio mergers. Top: the fraction of galaxies that host AGNs increases with galaxy stellar mass for major mergers (filled orange diamonds), minor mergers (filled green stars), and nonmergers (open black circles). The data on the x-axis are binned by 0.5 dex, and the points are offset on the x-axis for clarity. Bottom: the AGN excess, which is defined as the fraction of mergers that host AGNs over the fraction of nonmergers that host AGNs. The dashed line illustrates a ratio of 1, which means no difference between the fraction of mergers that host AGNs and the fraction of nonmergers that host AGNs. We observe AGN excess es for major mergers and minor mergers in the galaxy stellar mass bin $11 < \log(M_*/M_\odot) < 11.5$.

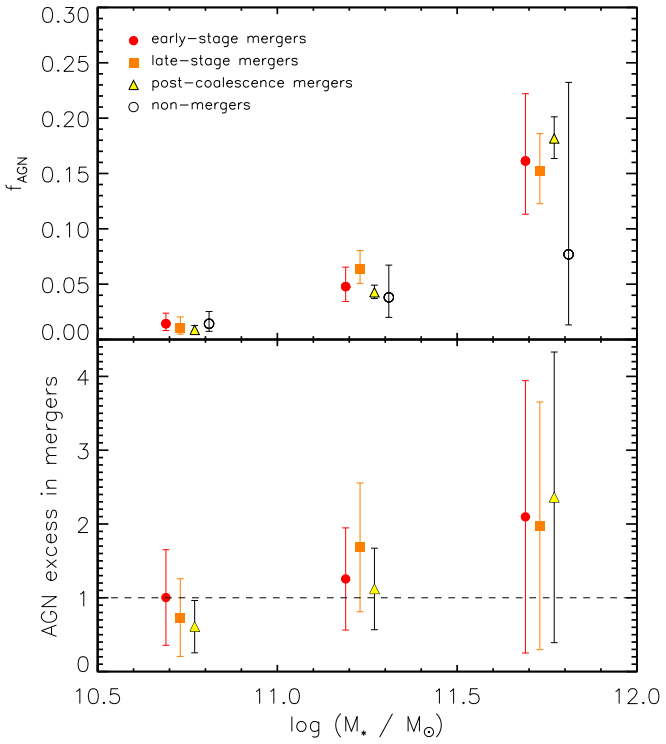

Figure 4. The fraction of galaxies that host AGNs and the AGN excess as a function of galaxy stellar mass, for different merger stages. Top: the fraction of galaxies that host AGNs increases with galaxy stellar mass for early-stage mergers (filled red circles), late-stage mergers (filled orange squares), post-coalescence mergers (filled yellow triangles), and nonmergers (open black circles). The data on the x-axis are binned by 0.5 dex, and the points are offset on the x-axis for clarity. Bottom: the AGN excess, which is defined as the fraction of mergers that host AGNs over the fraction of nonmergers that host AGNs. The dashed line illustrates a ratio of 1, which means no difference between the fraction of mergers that host AGNs and the fraction of nonmergers that host AGNs. The highest AGN excess we observe is for post-coalescence galaxy mergers in the most massive galaxy stellar mass bin ($11.5 < \log(M_*/M_\odot) < 12$), though it is still consistent with no excess to within the error bars.

strong correlation of AGN excess with galaxy-merger mass ratio, although they calculated their mass ratios using the stellar mass within the central 1 kpc of the galaxies instead of the total stellar mass of the galaxies, which prevents a direct comparison with our results. Further, in a study of mid-infrared-selected AGNs and BPT-selected AGNs in galaxy mergers (identified by a deep-learning convolutional neural network) in SDSS ($0.005 < z < 0.1$), Gao et al. (2020) found an AGN excess by a factor of up to 1.8 in mergers. In another SDSS study at $0.01 < z < 0.20$, Ellison et al. (2011; and, similarly, Ellison et al. 2013) used AGNs identified via BPT diagnostics and galaxy mergers identified via close pairs to uncover an AGN excess by a factor of up to 2.5 in mergers. They also found the strongest AGN excess in equal-mass galaxy pairs. With the close-pair sample in SDSS, Satyapal et al. (2014) found a similar excess using mid-infrared-selected AGNs. A different mid-infrared analysis of dusty AGNs in SDSS ($0.01 < z \leqslant 0.08$), which used visual identification of mergers, found an AGN excess by a factor of 2–7 in mergers (Weston et al. 2017).

5.2. An Excess of AGNs in Post-coalescence Galaxy Mergers of Stellar Mass $\sim 10^{12}$ M$_\odot$

Hydrodynamical simulations of galaxy mergers have predicted that AGN activity in mergers is preferentially triggered toward the end of the merger sequence, when the merger is funneling the most gas onto the AGNs (e.g., Van Wassenhove et al. 2012; Blecha et al. 2013; Capelo et al. 2017; Rosas-Guevara et al. 2019; McAlpine et al. 2020). Here, we test that prediction using the same galaxy stellar mass bins as in Section 5.1, and the same limiting AGN bolometric luminosity of $\log(L_{\rm bol}/{\rm erg\ s^{-1}}) > 44.4$ (Section 3.5). As Figure 4 shows, our results suggest that post-coalescence mergers have an AGN excess by a factor of 2.4, when compared to the AGN fraction in nonmergers, in the highest galaxy stellar mass bin that we consider ($11.5 < \log(M_*/M_\odot) < 12$). This is the highest AGN excess that we find of any merger stage in any galaxy stellar mass bin, though it is still consistent, within the error bars, with no excess.

Our measured AGN excess in post-coalescence mergers is broadly consistent with results from galaxy-pair observations, where the smallest-separation galaxy pairs trace the latest stages of galaxy mergers. A MaNGA analysis of AGNs in galaxy pairs also found that the fraction of AGNs increases with decreasing pair separation (Steffen et al. 2023). In that study, the AGNs were selected by BPT and WHAN diagnostics. Meanwhile, in another MaNGA study that classified AGNs by BPT and WHAN diagnostics, and galaxy-merger stages by a combination of kinematics and morphology, Jin et al. (2021) found no evolution of the AGN

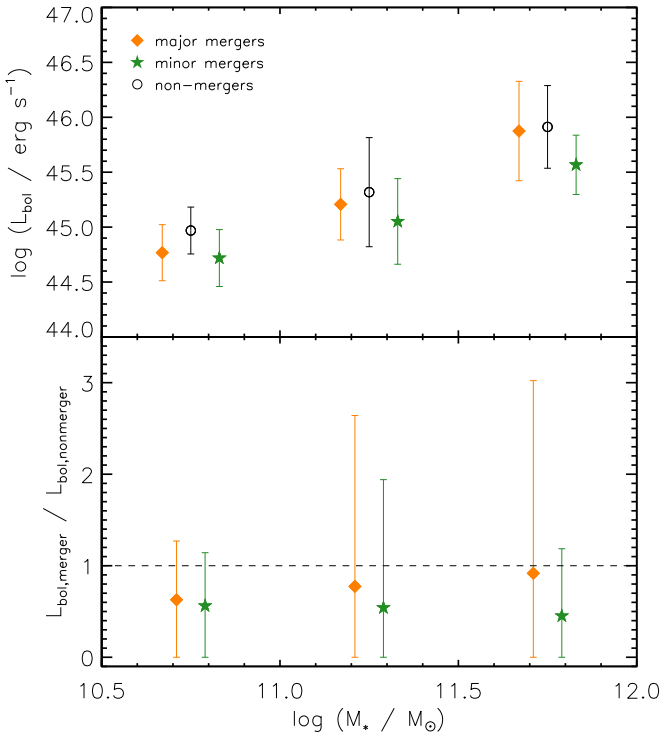

Figure 5. Top: mean bolometric luminosity of AGNs in major mergers (filled orange diamonds), minor mergers (filled green stars), and the mass-matched sample of AGNs in nonmergers (open black circles). Bottom: the ratio of the mean AGN bolometric luminosity in mergers to the mean AGN bolometric luminosity in mass-matched nonmergers, where the dashed horizontal line illustrates a ratio of 1. The AGNs analyzed have bolometric luminosities down to a limiting luminosity of $\log(L_{\rm bol}/{\rm erg\ s^{-1}}) > 44.4$. The data on the x-axis are binned by 0.5 dex, and the points are offset on the x-axis for clarity. While the well-known trend of increasing AGN luminosity with galaxy stellar mass is seen in all galaxy morphologies, there is no evidence for a luminosity dependence in AGN triggering in mergers.

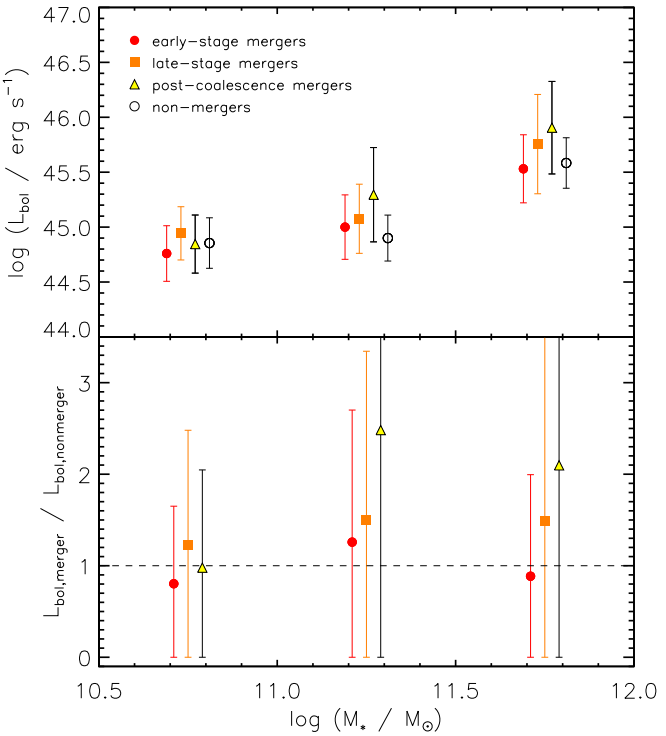

Figure 6. Top: mean bolometric luminosity of AGNs in early-stage mergers (filled red circles), late-stage mergers (filled orange squares), post-coalescence mergers (filled yellow triangles), and nonmergers (open black circles). Bottom: the ratio of the mean AGN bolometric luminosity in mergers to the mean AGN bolometric luminosity in mass-matched nonmergers, where the dashed horizontal line illustrates a ratio of 1. The AGNs analyzed have bolometric luminosities down to a limiting luminosity of $\log(L_{\rm bol}/{\rm erg\ s^{-1}}) > 44.4$. The data on the x-axis are binned by 0.5 dex, and the points are offset on the x-axis for clarity. While the mean AGN bolometric luminosities in post-coalescence mergers are elevated by a factor of ∼2–3 in the highest galaxy mass bins, they are still consistent within the errors with the mean AGN bolometric luminosities in nonmergers.

fraction across different merger sequences. The discrepancies between these MaNGA studies may be due to differing volume corrections and aperture sizes (e.g., Steffen et al. 2023). Studies of X-ray- and mid-infrared-selected AGNs in galaxy pairs also found that the fraction of AGNs increases as the pair separation decreases (e.g., Koss et al. 2012; Barrows et al. 2017; Stemo et al. 2021; Barrows et al. 2023), though these studies did not search for a galaxy mass dependence.

5.3. Higher-luminosity AGNs Are Not Preferentially Found in Mergers, Regardless of Merger Mass Ratio or Merger Stage

There is longstanding disagreement about whether galaxy mergers, or perhaps only certain types of mergers such as major mergers or post-coalescence mergers, more effectively drive gas onto SMBHs and trigger the most luminous AGNs (see, e.g., Storchi-Bergmann & Schnorr-Müller 2019 for a review). First, we test this by comparing the AGN bolometric luminosities in major mergers and minor mergers to nonmergers within the same mass bins. We use the same galaxy stellar mass bins as in Section 5.1 and the same limiting AGN bolometric luminosity of $\log(L_{\rm bol}/{\rm erg\ s^{-1}}) > 44.4$ (Section 3.5) for our analysis. The top panel of Figure 5 shows the known trend of AGN luminosity increasing with galaxy stellar mass, which we discussed in Section 3.5. More interestingly, that figure also shows that the mean AGN bolometric luminosity is roughly the same for major mergers, minor mergers, and nonmergers in the same galaxy mass bin. We find no evidence for major mergers or minor mergers preferentially triggering higher-luminosity AGNs.

Our result is in agreement with previous studies that used infrared and/or X-ray selectors of AGNs (e.g., Kocevski et al. 2012; Villforth et al. 2014; Barrows et al. 2017; Villforth et al. 2017; Stemo et al. 2021). In contrast, other studies of AGNs in SDSS and in MaNGA found that the [O III] luminosities of AGNs are ∼0.13–0.5 dex higher in mergers than in nonmergers (Ellison et al. 2013; Jin et al. 2021). These studies used BPT-based AGN identifications, which are prone to misclassifications, as discussed in Section 5.1; further, [O III] bolometric corrections depend on factors such as luminosity and the ionization state of the gas (e.g., Netzer 2009). These effects may contribute to the difference in our results.

Next, we consider the AGN luminosity as a function of merger stage. While the AGNs in post-coalescence mergers of high-stellar-mass galaxies ($11 < \log(M_*/M_\odot) < 12$) seem to have bolometric luminosities that are ∼2–3 times larger, on average, than those of AGNs in nonmergers of the same mass range, it is not a statistically significant result (Figure 6). If real, this hint of a correlation would match findings that post-merger galaxies have more enhanced AGN luminosities than other merger stages (e.g., Ellison et al. 2013), but within the error bars our results are consistent with other studies that found no

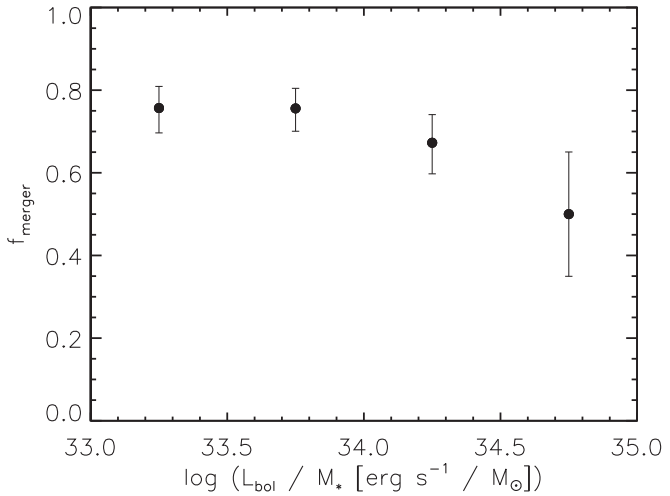

Figure 7. Fraction of AGNs in mergers as a function of the ratio of AGN bolometric luminosity to the host-galaxy stellar mass, which is a proxy for the Eddington ratio. The AGNs analyzed have bolometric luminosities down to a limiting luminosity of $\log(L_{bol}/\mathrm{erg\ s^{-1}}) > 44.4$. The data on the x-axis are binned by 0.5 dex. Within the error bars, we find no significant evidence for mergers preferentially triggering lower or higher Eddington ratios.

evolution of AGN luminosity with merger stage (e.g., Steffen et al. 2023).

5.4. Galaxy Mergers Do Not Trigger Higher SMBH Accretion Rates

While we find an excess of AGNs in higher-mass galaxy mergers (Sections 5.1 and 5.2), we now consider whether these galaxy mergers enhance the accretion efficiencies onto the SMBHs. Here, we use the ratio of the AGN bolometric luminosity to the host-galaxy stellar mass, L_{bol}/M_*, as a proxy for the Eddington ratio. Using the same limiting AGN bolometric luminosity of $\log(L_{bol}/\mathrm{erg\ s^{-1}}) > 44.4$ (Section 3.5), and bins of 0.5 dex centered at $\log[(L_{bol}/M_*)(\mathrm{erg\ s^{-1}}/M_\odot)] = [33.25, 33.75, 34.25, 34.75]$, we measure f_{merger} in each bin. The merger fraction, f_{merger}, is defined as the number of AGNs in mergers divided by the number of AGNs in each bin. We find no significant trend of a dependence of f_{merger} on Eddington ratio (traced by L_{bol}/M_*), as shown in Figure 7.

Our results are consistent with simulations and phenomenological models that found no significant differences in the Eddington ratios of AGNs in galaxy mergers (Steinborn et al. 2016; Weigel et al. 2018; McAlpine et al. 2020). In addition, observations of WISE AGNs in galaxy pairs also reported no significant correlation of the AGN merger fraction with L_{bol}/M_* (Barrows et al. 2023). A further study of broad-line AGNs at $z \sim 2$ also found that major mergers do not correlate with high-accretion AGNs (Marian et al. 2019). We conclude that galaxy mergers do not trigger higher accretion rates of material onto SMBHs for AGNs with $\log(L_{bol}/\mathrm{erg\ s^{-1}}) > 44.4$.

6. Conclusions

We present identifications of 387 unique AGNs in the full, final catalog of MaNGA galaxies. We identified these AGNs by their WISE colors, Swift/BAT ultra-hard X-ray sources, NVSS/FIRST radio observations, and/or broad emission lines. We combined these AGN identifications with MaNGA galaxy-merger classifications, where the galaxy morphologies are derived from a linear discriminant analysis of seven individual imaging predictors (Gini, M_{20}, concentration, asymmetry, clumpiness, Sérsic index, and shape asymmetry) that were measured for mock SDSS r-band images of simulated merging and isolated galaxies (Nevin et al. 2023). These galaxy classifications included major and minor mergers, as well as early-stage, late-stage, and post-coalescence mergers, enabling us to examine the roles of various types and stages of mergers in triggering or enhancing AGN activity.

For the analyses in this paper, we applied a limiting AGN bolometric luminosity of $\log(L_{bol}/\mathrm{erg\ s^{-1}}) > 44.4$, above which all four approaches can detect an AGN. This luminosity cutoff decreased our AGN sample size from 387 to 301. Our main results for this AGN sample are summarized below.

1. Overall, we find that $4.2\% \pm 0.3\%$ (168/3969) of MaNGA galaxy mergers host AGNs with $\log(L_{bol}/\mathrm{erg\ s^{-1}}) > 44.4$ and $1.8\% \pm 0.2\%$ (66/3700) of MaNGA nonmergers host AGNs with $\log(L_{bol}/\mathrm{erg\ s^{-1}}) > 44.4$.

2. This AGN fraction is correlated with host-galaxy mass, and we find an excess of AGNs in mergers (relative to nonmergers) for major mergers (excess by a factor of 1.8) and minor mergers (excess by a factor of 1.5) in the galaxy stellar mass bin $11 < \log(M_*/M_\odot) < 11.5$ (Figure 3). Overall, the AGN excess trends somewhat stronger in major mergers than in minor mergers.

3. When we sort by merger stage, we find the highest AGN excess (relative to nonmergers) for post-coalescence mergers in the highest-stellar-mass galaxies in MaNGA ($11.5 < \log(M_*/M_\odot) < 12$). This factor of 2.4 excess has large error bars, and is also consistent with no excess (Figure 4).

4. We find no evidence for different merger types or merger stages preferentially triggering higher-luminosity AGNs. AGNs in major mergers and minor mergers have comparable luminosities to AGNs in nonmergers (Figure 5), and AGNs in early-stage, late-stage, and post-coalescence mergers also have similar luminosities to AGNs in nonmergers (Figure 6).

5. There is no correlation of the merger fraction, which is the ratio of the number AGNs in mergers to the number of AGNs, with Eddington ratio (Figure 7). We find that an AGN is ∼equally like to be found in a merger, regardless of the accretion rate, indicating that galaxy mergers do not enhance the efficiency of accretion onto SMBHs.

In conclusion, we find that AGNs with bolometric luminosities $\log(L_{bol}/\mathrm{erg\ s^{-1}}) > 44.4$ are more likely to be triggered or enhanced in galaxy mergers than in nonmergers, for galaxies of stellar mass $\sim 10^{11-12}\,M_\odot$ in MaNGA. Although AGNs are more likely to be present in these galaxy mergers, the luminosities and accretion rates of these AGNs are, on average, no different than those of AGNs in nonmerging galaxies. Observations of the molecular gas content of the host galaxies could further clarify whether there is correspondingly no difference in the gas available for accretion onto SMBHs in the merging galaxies as opposed to the nonmerging galaxies.

Acknowledgments

J.M.C. is supported by NSF AST-1714503 and NSF AST-1847938. R.N. is supported by NSF AST-1714503. J.N. is supported by NSF AST-1847938. A.M.S. is supported by a National Science Foundation MPS-Ascend Postdoctoral Research Fellowship under grant No. 2213288.

Funding for the Sloan Digital Sky Survey-IV has been provided by the Alfred P. Sloan Foundation, the U.S.

Department of Energy Office of Science, and the Participating Institutions. SDSS-IV acknowledges support and resources from the Center for High-Performance Computing at the University of Utah. The SDSS website is www.sdss.org.

SDSS-IV is managed by the Astrophysical Research Consortium for the Participating Institutions of the SDSS Collaboration including the Brazilian Participation Group, the Carnegie Institution for Science, Carnegie Mellon University, the Chilean Participation Group, the French Participation Group, Harvard-Smithsonian Center for Astrophysics, Instituto de Astrofísica de Canarias, The Johns Hopkins University, Kavli Institute for the Physics and Mathematics of the Universe (IPMU) / University of Tokyo, the Korean Participation Group, Lawrence Berkeley National Laboratory, Leibniz Institut für Astrophysik Potsdam (AIP), Max-Planck-Institut für Astronomie (MPIA Heidelberg), Max-Planck-Institut für Astrophysik (MPA Garching), Max-Planck-Institut für Extraterrestrische Physik (MPE), National Astronomical Observatories of China, New Mexico State University, New York University, University of Notre Dame, Observatário Nacional / MCTI, The Ohio State University, Pennsylvania State University, Shanghai Astronomical Observatory, United Kingdom Participation Group, Universidad Nacional Autónoma de México, University of Arizona, University of Colorado Boulder, University of Oxford, University of Portsmouth, University of Utah, University of Virginia, University of Washington, University of Wisconsin, Vanderbilt University, and Yale University. This project makes use of the MaNGA-Pipe3D dataproducts. We thank the IA-UNAM MaNGA team for creating this catalog, and the Conacyt Project CB-285080 for supporting them.

ORCID iDs

Rebecca Nevin https://orcid.org/0000-0003-1056-8401
James Negus https://orcid.org/0000-0003-2667-7645
R. Scott Barrows https://orcid.org/0000-0002-6212-7328
Michael Eracleous https://orcid.org/0000-0002-3719-940X
Namrata Roy https://orcid.org/0000-0002-4430-8846
Aaron Stemo https://orcid.org/0000-0003-1542-0799
Thaisa Storchi-Bergmann https://orcid.org/0000-0003-1772-0023
Dominika Wylezalek https://orcid.org/0000-0003-2212-6045

References

Abdurro'uf, Accetta, K., Aerts, C., et al. 2022, ApJS, 259, 35
Alam, S., Albareti, F. D., Allende Prieto, C., et al. 2015, ApJS, 219, 12
Albán, M., & Wylezalek, D. 2023, A&A, 674, A85
Araujo, B. L. C., Storchi-Bergmann, T., Rembold, S. B., Kaipper, A. L. P., & Dall'Agnol de Oliveira, B. 2023, MNRAS, 522, 5165
Assef, R. J., Stern, D., Noirot, G., et al. 2018, ApJS, 234, 23
Baldwin, J. A., Phillips, M. M., & Terlevich, R. 1981, PASP, 93, 5
Barnes, J. E., & Hernquist, L. 1992, ARA&A, 30, 705
Barnes, J. E., & Hernquist, L. E. 1991, ApJL, 370, L65
Barrows, R. S., Comerford, J. M., Greene, J. E., & Pooley, D. 2016, ApJ, 829, 37
Barrows, R. S., Comerford, J. M., Greene, J. E., & Pooley, D. 2017, ApJ, 838, 129
Barrows, R. S., Comerford, J. M., Stern, D., & Assef, R. J. 2021, ApJ, 922, 179
Barrows, R. S., Comerford, J. M., Stern, D., & Assef, R. J. 2023, ApJ, 951, 92
Baum, S. A., Heckman, T. M., & van Breugel, W. 1992, ApJ, 389, 208
Becker, R. H., White, R. L., & Helfand, D. J. 1995, ApJ, 450, 559
Best, P. N., & Heckman, T. M. 2012, MNRAS, 421, 1569
Best, P. N., Kauffmann, G., Heckman, T. M., & Ivezić, Ž. 2005, MNRAS, 362, 9
Bickley, R. W., Bottrell, C., Hani, M. H., et al. 2021, MNRAS, 504, 372
Blanton, M. R., Bershady, M. A., Abolfathi, B., et al. 2017, AJ, 154, 28
Blecha, L., Loeb, A., & Narayan, R. 2013, MNRAS, 429, 2594
Bournaud, F., & Combes, F. 2002, A&A, 392, 83
Bundy, K., Bershady, M. A., Law, D. R., et al. 2015, ApJ, 798, 7
Canalizo, G., & Stockton, A. 2001, ApJ, 555, 719
Capelo, P. R., Dotti, M., Volonteri, M., et al. 2017, MNRAS, 469, 4437
Capelo, P. R., Volonteri, M., Dotti, M., et al. 2015, MNRAS, 447, 2123
Cid Fernandes, R., Stasińska, G., Schlickmann, M. S., et al. 2010, MNRAS, 403, 1036
Cisternas, M., Jahnke, K., Inskip, K. J., et al. 2011, ApJ, 726, 57
Combes, F., & Gerin, M. 1985, A&A, 150, 327
Comerford, J. M., Negus, J., Müller-Sánchez, F., et al. 2020, ApJ, 901, 159
Comerford, J. M., Pooley, D., Barrows, R. S., et al. 2015, ApJ, 806, 219
Condon, J. J., Cotton, W. D., Greisen, E. W., et al. 1998, AJ, 115, 1693
Di Matteo, T., Springel, V., & Hernquist, L. 2005, Natur, 433, 604
Drory, N., MacDonald, N., Bershady, M. A., et al. 2015, AJ, 149, 77
Dunlop, J. S., McLure, R. J., Kukula, M. J., et al. 2003, MNRAS, 340, 1095
Ellison, S. L., Mendel, J. T., Patton, D. R., & Scudder, J. M. 2013, MNRAS, 435, 3627
Ellison, S. L., Patton, D. R., Mendel, J. T., & Scudder, J. M. 2011, MNRAS, 418, 2043
Ellison, S. L., Viswanathan, A., Patton, D. R., et al. 2019, MNRAS, 487, 2491
Elvis, M., Wilkes, B. J., McDowell, J. C., et al. 1994, ApJS, 95, 1
Ferrarese, L., & Ford, H. 2005, SSRv, 116, 523
Fu, H., Steffen, J. L., Gross, A. C., et al. 2018, ApJ, 856, 93
Gabor, J. M., Impey, C. D., Jahnke, K., et al. 2009, ApJ, 691, 705
Gao, F., Wang, L., Pearson, W. J., et al. 2020, A&A, 637, A94
Glikman, E., Simmons, B., Mailly, M., et al. 2015, ApJ, 806, 218
Hopkins, P. F., & Hernquist, L. 2009, ApJ, 694, 599
Hopkins, P. F., Kocevski, D. D., & Bundy, K. 2014, MNRAS, 445, 823
Ichikawa, K., Ricci, C., Ueda, Y., et al. 2019, ApJ, 870, 31
Jin, G., Dai, Y. S., Pan, H.-A., et al. 2021, ApJ, 923, 6
Kauffmann, G., Heckman, T. M., & Best, P. N. 2008, MNRAS, 384, 953
Kewley, L. J., Dopita, M. A., Leitherer, C., et al. 2013, ApJ, 774, 100
Kewley, L. J., Groves, B., Kauffmann, G., & Heckman, T. 2006, MNRAS, 372, 961
Kocevski, D. D., Faber, S. M., Mozena, M., et al. 2012, ApJ, 744, 148
Kormendy, J., & Richstone, D. 1995, ARA&A, 33, 581
Koss, M., Mushotzky, R., Treister, E., et al. 2012, ApJL, 746, L22
Law, D. R., Yan, R., Bershady, M. A., et al. 2015, AJ, 150, 19
Lynden-Bell, D. 1979, MNRAS, 187, 101
Magorrian, J., Tremaine, S., Richstone, D., et al. 1998, AJ, 115, 2285
Mainzer, A., Bauer, J., Cutri, R. M., et al. 2014, ApJ, 792, 30
Marconi, A., Risaliti, G., Gilli, R., et al. 2004, MNRAS, 351, 169
Marian, V., Jahnke, K., Mechtley, M., et al. 2019, ApJ, 882, 141
McAlpine, S., Harrison, C. M., Rosario, D. J., et al. 2020, MNRAS, 494, 5713
Mendez, A. J., Coil, A. L., Aird, J., et al. 2013, ApJ, 770, 40
Netzer, H. 2009, MNRAS, 399, 1907
Nevin, R., Blecha, L., Comerford, J., & Greene, J. 2019, ApJ, 872, 76
Nevin, R., Blecha, L., Comerford, J., et al. 2023, MNRAS, 522, 1
Oh, K., Koss, M., Markwardt, C. B., et al. 2018, ApJS, 235, 4
Oh, K., Yi, S. K., Schawinski, K., et al. 2015, ApJS, 219, 1
Osterbrock, D. E. 1991, RPPh, 54, 579
Panessa, F., Tarchi, A., Castangia, P., et al. 2015, MNRAS, 447, 1289
Patton, D. R., Pritchet, C. J., Carlberg, R. G., et al. 2002, ApJ, 565, 208
Pennell, A., Runnoe, J. C., & Brotherton, M. S. 2017, MNRAS, 468, 1433
Pierce, J. C. S., Tadhunter, C., Ramos Almeida, C., et al. 2023, MNRAS, 522, 1736
Ricci, C., Trakhtenbrot, B., Koss, M. J., et al. 2017, ApJS, 233, 17
Rich, J. A., Kewley, L. J., & Dopita, M. A. 2011, ApJ, 734, 87
Rosas-Guevara, Y. M., Bower, R. G., McAlpine, S., Bonoli, S., & Tissera, P. B. 2019, MNRAS, 483, 2712
Sánchez, S. F., Avila-Reese, V., Hernandez-Toledo, H., et al. 2018, RMxAA, 54, 217
Sánchez, S. F., Pérez, E., Sánchez-Blázquez, P., et al. 2016, RMxAA, 52, 171
Satyapal, S., Ellison, S. L., McAlpine, W., et al. 2014, MNRAS, 441, 1297
Snyder, G. F., Lotz, J. M., Rodriguez-Gomez, V., et al. 2017, MNRAS, 468, 207
Springel, V., Di Matteo, T., & Hernquist, L. 2005, ApJL, 620, L79
Steffen, J. L., Fu, H., Brownstein, J. R., et al. 2023, ApJ, 942, 107
Steinborn, L. K., Dolag, K., Comerford, J. M., et al. 2016, MNRAS, 458, 1013
Stemo, A., Comerford, J. M., Barrows, R. S., et al. 2021, ApJ, 923, 36
Stern, D. 2015, ApJ, 807, 129
Storchi-Bergmann, T., & Schnorr-Müller, A. 2019, NatAs, 3, 48

Treister, E., Schawinski, K., Urry, C. M., & Simmons, B. D. 2012, ApJL, 758, L39
Van Wassenhove, S., Volonteri, M., Mayer, L., et al. 2012, ApJL, 748, L7
Véron-Cetty, M. P., & Véron, P. 2001, A&A, 375, 791
Villar-Martín, M., Tadhunter, C., Humphrey, A., et al. 2011, MNRAS, 416, 262
Villforth, C., Hamann, F., Rosario, D. J., et al. 2014, MNRAS, 439, 3342
Villforth, C., Hamilton, T., Pawlik, M. M., et al. 2017, MNRAS, 466, 812
Wake, D. A., Bundy, K., Diamond-Stanic, A. M., et al. 2017, AJ, 154, 86
Weigel, A. K., Schawinski, K., Treister, E., Trakhtenbrot, B., & Sanders, D. B. 2018, MNRAS, 476, 2308
Weston, M. E., McIntosh, D. H., Brodwin, M., et al. 2017, MNRAS, 464, 3882
Wright, E. L., Eisenhardt, P. R. M., Mainzer, A. K., et al. 2010, AJ, 140, 1868
Yan, R., Bundy, K., Law, D. R., et al. 2016, AJ, 152, 197